Investigation of Leakage Flow and Heat Transfer in a Gas Turbine Blade Tip With Emphasis on the Effect of Rotation

Dianliang Yang

Xiaobing Yu

Zhenping Feng
e-mail: zpfeng@mail.xjtu.edu.cn

Institute of Turbomachinery,
Xi'an Jiaotong University,
Xi'an 710049, P.R.C.

Numerical analysis was applied to investigate the effect of rotation on the blade tip leakage flow and heat transfer. Flows around both flat and squealer tips at the first stage rotor blade of GE E^3 high-pressure turbine were studied. The tip gap and squealer groove depth were specified as 1% and 2% of the blade height, respectively. The heat transfer coefficient on the tip surface was obtained by using different turbulence models and compared with the experimental data. The grid independence study was also carried out by using the Richardson extrapolation method. The effect of the blade rotation was studied in the following cases: (1) the blade domain is rotating and the shroud is stationary; (2) the blade domain is stationary and the shroud is rotating; and (3) both blade domain and shroud are stationary. In this approach, the effects of the relative motion of the endwall, the centrifugal force, and the Coriolis force can be investigated, respectively. By comparing the results of the three cases discussed, it is concluded that the main effect of the rotation on the tip leakage flow and heat transfer resulted from the relative motion of the shroud, especially for the squealer tip blade. [DOI: 10.1115/1.3213560]

1 Introduction

In order to increase the efficiency and power output, modern gas turbines inlet temperature is increased continually, which results in high heat loads on the turbines' "hot" components. Many studies have been done on airfoil heat transfer in higher temperature regions. Dozens of cooling techniques have been applied to reduce the high heat load and to ensure blade life cycle. However, there still exist some problems that need to be investigated, such as the heat transfer and cooling of the rotor blade tip. In modern gas turbine engines, unshrouded blade failures caused by the high heat transfer rates near the tip region are still away from solved. For unshrouded rotor blades, there is a gap between the rotating blade tip and the stationary casing. Driven by the large pressure difference between the blade pressure and suction sides, the leakage flow will be accelerated in the tip gap region and impinge on the blade tip to cause a high heat transfer region. Therefore, the blade tip can be one of the regions with the highest heat transfer rate on the entire blade surface. Typically, the blade tip is grooved chordwise in order to reduce the tip leakage flow, as it is called "squealer tip." The groove acts as a labyrinth seal to increase the flow resistance and thus reduces the leakage flow.

The early studies on the blade tip heat transfer have been summarized by Bunker [1]. These studies were performed by using the scaled models of the blade tip. The earliest study on the blade tip heat transfer was done by Mayle and Metzger [2]. They studied the tip heat transfer by using a 2D rectangular tip model with and without a rotating shroud. Later, Metzger and Bunker et al. [3] measured the local convective heat transfer for the case of flow through a narrow slot-type channel with a rectangular groove. Chyu et al. [4] carried out a study with a similar structure but without a moving shroud wall. They noted that the relative motion of the shroud has a minor effect on the tip averaged heat transfer coefficient.

In the last decade, linear cascades were adopted to obtain the tip flow and heat transfer characteristics for the flat and squealer tips. Bunker et al. [5] first obtained the detailed heat transfer coefficient distributions on a large power generation turbine blade tip under the engine representative flow conditions. The results show that only certain regions of the linear cascade tip appear to conform to a simple pressure driven heat transfer behavior similar to that of the modeled blade tip, but with significant local modifications due to the three-dimensional nature of the flow. Later, Azad et al. [6,7] and Kwak and Han [8,9] reported the experimental results of the flat and squealer tips of the GE E^3 first stage rotor blade with the different boundary conditions. They studied the effects of the turbulence intensity, the tip gap height, and the tip geometry on the tip heat transfer. They reported that the heat transfer distribution on the flat tip is similar to that obtained by Bunker et al. [5]. By comparing with the flat tip, the heat transfer distribution on the squealer tip changes and the averaged tip heat transfer coefficient reduces. Newton et al. [10] measured the heat transfer coefficient near the tip region of a generic turbine blade in a five-blade linear cascade. The experiment reveals that the flow through the flat tip is dominated by the flow separation at the pressure side edge. The highest level of the heat transfer is located where the flow reattaches on the tip surface. Nasir et al. [11] gave the same conclusions with similar blade geometry.

It is difficult to measure flows and heat transfer in the tip gap region, especially for the rotating blades. However, in order to design an optimal cooling scheme, it is important to have a good understanding of the complex flow field in the tip gap and the effect of the blade rotation on the tip heat transfer.

With the development of computational technology, computational fluid dynamics (CFD) has played an increasingly important role in the blade tip leakage flow and heat transfer studies. Ameri and Bunker [12] first performed a numerical simulation to investigate the detailed distribution of the convective heat transfer coefficient on the blade tip surface in a large power generation turbine. By using the k-ω low Reynolds number turbulence model and more than 1.2×10^6 grids, the results showed that a good representation of the tip heat transfer can be made by those numerical methods. Yang et al. [13,14] reported the numerical re-

Contributed by the International Gas Turbine Institute of ASME for publication in the JOURNAL OF TURBOMACHINERY. Manuscript received April 1, 2009; final manuscript received April 21, 2009; published online May 4, 2010. Review conducted by David Wisler. Paper presented at the ASME Turbo Expo 2008: Land, Sea and Air (GT2008), Berlin, Germany, June 9–13, 2008.

sults of the GE E^3 high-pressure turbine rotor blade with flat and squealer tips. They pointed out that the best agreement in the peak value could be obtained by using the RNG k-ε model for the flat tip blade, and the Reynolds stress model for the squealer tip blade. Mumic et al. [15] simulated the tip leakage flow and heat transfer similar to that of Yang's model by using the low Re shear stress transport (SST) k-ω model. The predicted tip heat transfer and static pressure distributions showed reasonable agreement with the experimental data. The flat blade tip provides a higher overall heat transfer coefficient than the squealer blade tip.

There have already been a number of data in the open literature on the rotating blade tip heat transfer. Ameri et al. [16] simulated the tip flow and heat transfer on the GE E^3 first stage rotor blade first. Yang and Feng [17] performed the numerical investigation by using the similar blade structure in different tip gap heights and groove depths. All of these studies indicated that the flow structure and heat transfer distribution in the linear cascade are different from that in the rotating blade. Also, some researchers have performed the time-resolved investigations on the tip heat transfer in full turbine stage [18–20], showing that there is a significant unsteady impact to the tip heat transfer coefficient.

However, few studies have focused on the effect of the blade rotation. Rhee and Cho [21,22] investigated the local heat/mass transfer characteristics on the flat tip by using a low speed rotating turbine annular cascade. They pointed out that when the blade rotates, the heat/mass transfer enhanced region on the tip is shifted toward the downstream side, and the level of heat/mass transfer coefficients at the upstream region of the tip is slightly decreased due to the reduced tip gap flow with rotation. Palafox et al. [23,24] investigated the leakage flow structure and heat transfer on the tip in a very large-scale linear cascade with a stationary or moving endwall. They stated that the relative endwall motion has an obvious influence on both the leakage flow and heat transfer distribution on the tip. Krishnababu et al. [25] studied the effect of the casing motion on the tip leakage flow and heat transfer characteristics. The effect of the relative casing motion was to reduce the tip leakage mass flow rate. The averaged heat transfer rate on the blade tip was reduced as the leakage flow velocity decreases due to drop of the driven pressure difference.

In this paper, numerical investigations were performed to study the effect of the blade rotation in the flat and squealer tips. The effect of the blade rotation consists of two aspects: one is the relative motion between the blade tip and the endwall, another is the centrifugal and Coriolis forces. These effects result in the difference in the leakage flow and the heat transfer between the stationary and rotating blade tips. The effects of the two factors will be discussed in detail in this paper.

2 Research Methods

All of the numerical simulations are performed in the relative coordinate frame. Additional sources from blade rotating with a constant angular speed are added to the momentum and energy equations to account for the Coriolis and centrifugal forces. To this end, the effects of the Coriolis and centrifugal forces on the tip leakage flow and heat transfer can be analyzed by comparing the stationary and rotating cases with the same domain grids and boundary conditions.

In this paper, three computational cases are presented as follows: (1) blade domain is rotating and shroud is stationary (DRSS); (2) blade domain is stationary and shroud is rotating (DSSR); and (3) both blade domain and shroud are stationary (DSSS). The comparison between DRSS and DSSR can be used to reveal the effect of the centrifugal and Coriolis forces, while the comparison between DSSR and DSSS can be used to study the effect of the relative motion of the endwall.

3 Computation Details

The blade geometry is the first stage rotor blade in GE E^3 engine's high-pressure turbine. The detailed blade geometry and operating conditions can be found in Ref. [26]. In this paper, both the flat and squealer tips are studied with 1% tip gap clearance. For the flat tip case, the tip surface of the rotor blade is cylindrical. For the squealer tip case, the groove depth is specified as 2% of the blade height and the squealer tip sidewall thickness is 0.77 mm.

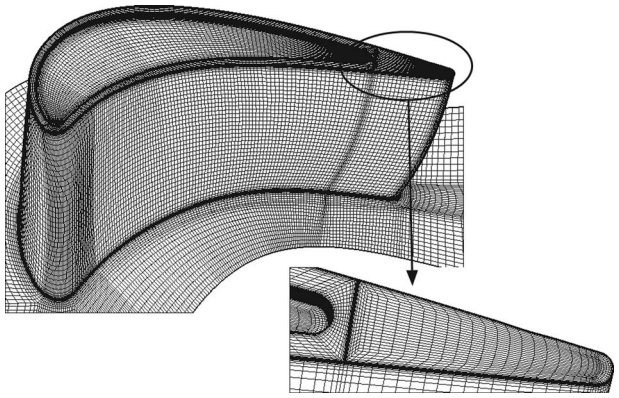

Fig. 1 Grid distribution for the squealer tip

The numerical simulations are performed by using a commercial CFD software CFX5.7. The solutions are obtained by solving the steady compressible Reynolds-averaged Navier–Stokes equations, discretized with a finite control volume method. The overall solution accuracy is of the second order. The software ICEMCFD is employed to generate the structured grids in the computational domain. H-type grid is used for blade passage, while O-type grid is used for the regions around the blade surface and tip gap entrance for higher grid quality. The low Reynolds k-ω two-equation turbulence model is employed.

As low Reynolds number k-ω model requires $y^+ < 2$ at least, the wall grid y^+ is about 0.5 for all cases in this paper. A large number of grid nodes are placed near the solid walls to obtain proper resolution of the boundary layer flow. In the current study, calculations are performed with about 1.5×10^6 grid nodes for the flat tip blade cases and 1.8×10^6 grid nodes for the squealer tip blade cases. Figure 1 shows the grid generation result of the squealer tip blade.

The computations are carried out within a single blade passage with the periodic boundary conditions imposed along the pitch direction. A numerical simulation on the DRSS case is performed first, and its boundary conditions can be found in Ref. [17]. When convergence is reached, the relative inlet boundary conditions of the DRSS case, including the total pressure, total temperature, and inlet angles, are set to the absolute inlet boundary conditions for the DSSR and DSSS cases. The static pressure boundary condition, which is the same as that for the DRSS case, is specified as the outlet boundary condition for the DSSR and DSSS cases. Therefore, the same boundary conditions are used for these simulations in the relative coordinate frame. Figure 2 shows the detailed boundary conditions obtained from the convergence solutions for three cases. For the DSSR case, the endwall rotates at 8450 rpm from the suction side to the pressure side of the blade. In all cases, wall temperature is specified as 496 K.

In order to validate the ability of the different turbulence models to the present study, a linear cascade studied by Kwak [9] is calculated first. The case is a flat tip blade with a 1.5% tip gap clearance. Four turbulence models are used, which includes two high Re models (standard k-ε and RNG k-ε) and two low Re models (low Re k-ω and SST k-ω).

Figure 3 shows the comparison of the tip heat transfer coefficient between the measured and predicted results. It indicates that the distribution of the heat transfer coefficient on the blade tip can be predicted well by all of the turbulence models. But the computed magnitude is overpredicted by all of the high Reynolds

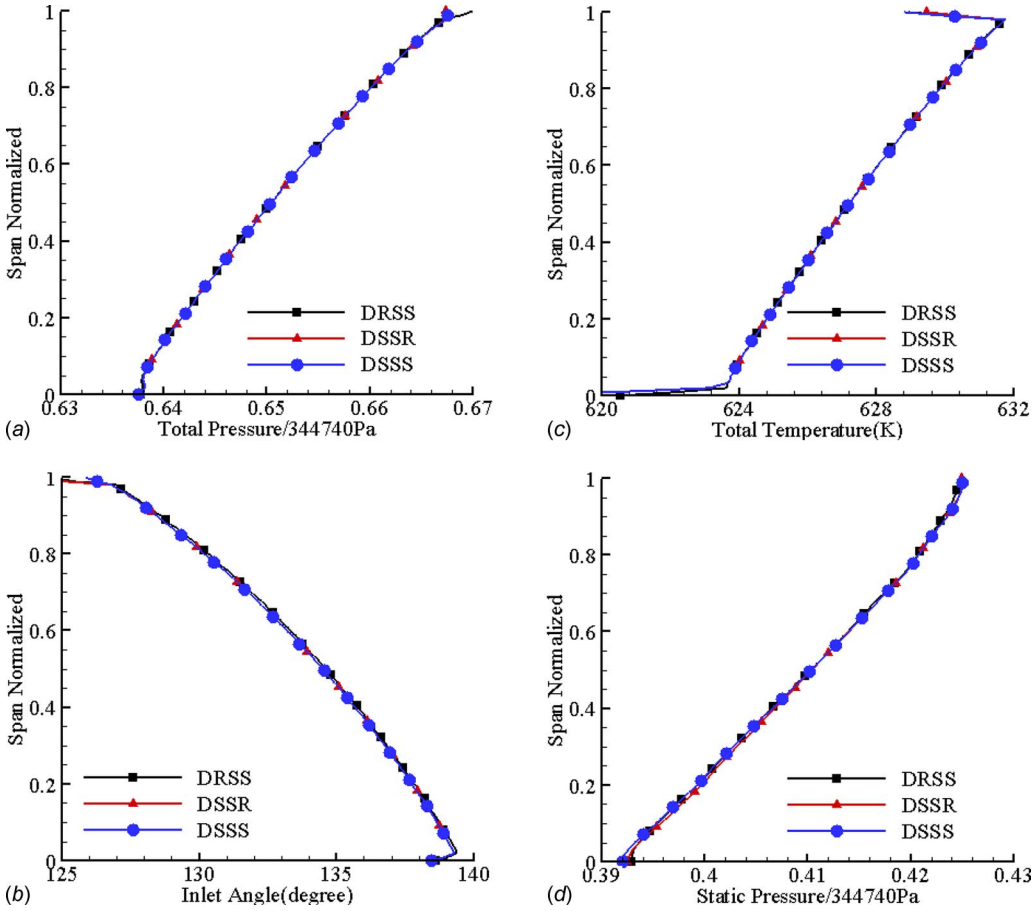

Fig. 2 Detailed boundary conditions for all cases: (*a*) inlet total pressure, (*b*) inlet total temperature, (*c*) inlet angle, and (*d*) outlet static pressure

number turbulence models based on the ε equation, especially for the standard k-ε turbulence model. The computed magnitude is underpredicted by the SST k-ω turbulence model after the 30% axial chord. The results with the low Re k-ω turbulence model match best with the test data.

Four different meshes with resolution of 0.8×10^6, 1.1×10^6, 1.47×10^6, and 2.57×10^6 grid nodes are used to have grid-independence solution. The mesh refinement is imposed in three coordinate directions synchronously for every mesh. The tip gap clearance of the test cases is specified as 1% of the blade height. The low Re k-ω two-equation turbulence model is employed. The wall grid y^+ is less than 1 for all meshes.

Figure 4 shows that the distributions of the heat transfer coefficient on the tip and the surface streamlines near the tip. A division line can be found along the pressure side on the tip. A separation vortex exists between the division line and the pressure side. The re-attached flow results in the high heat transfer coefficient near the division line. There exists the similar flow structure and heat transfer distribution in different grid numbers. Also, the increasing grid number has a limited influence on the position of the division line.

The area-averaged heat transfer coefficients (h) on the blade tip obtained by the different meshes are shown in Table 1. By using the Richardson extrapolation method, an extrapolation value is obtained from the results with 1.47×10^6 grid nodes and 2.57×10^6 grid nodes to study numerical results. The heat transfer coefficient from the Richardson extrapolation is 933.209 $\mathrm{W/m^2\,K}$. As a second order upwind scheme is used to discretize the convection term in this paper, therefore, the averaged heat transfer coefficient from the Richardson extrapolation has a third order accuracy based on Roache's investigation [27]. It is assumed that this coefficient is the baseline solution. The relative error of the heat transfer coefficient is 2.26% for the solution with 0.8×10^6 grid nodes, and it reduces to 0.8% for the solution with 2.57×10^6 grid nodes. The error for the solution with 1.47×10^6 grid nodes is very close to that with 2.57×10^6 grid nodes. Therefore, a mesh with about 1.5×10^6 grid nodes is used to study the flat tip heat transfer in this paper.

4 Results and Discussion

4.1 Flat Tip. Since the blade tip clearance is usually very small, the relative motion of the endwall has significant effect on the leakage flow through the tip gap. The leakage flow, which is approximately vertical to the camber line of the blade tip, has a large value of circumferential velocity component. So the centrifugal and Coriolis forces will also affect the leakage flow.

Figure 5 shows the secondary flow streamlines at various axial locations around the flat tip. The ordinate in Fig. 5 is enlarged five times in spanwise direction for clarity.

At the 20% axial chord location, the endwall relative motion can block the leakage flow for the DRSS and DSSR cases. At the exit area of the tip gap near the suction side, the leakage flow is pushed to the blade tip surface by the boundary layer flow, and only a small quantity of gas can go through the tip gap. It seems that the effect of the scraping flow in the tip gap is more pronounced for the DRSS case. It takes about 70% tip height at the exit area of the tip gap in the DRSS case, but only 50% tip height in the DSSR case. The difference shows the effect of the centrifugal and Coriolis forces. Since the endwall relative velocity is

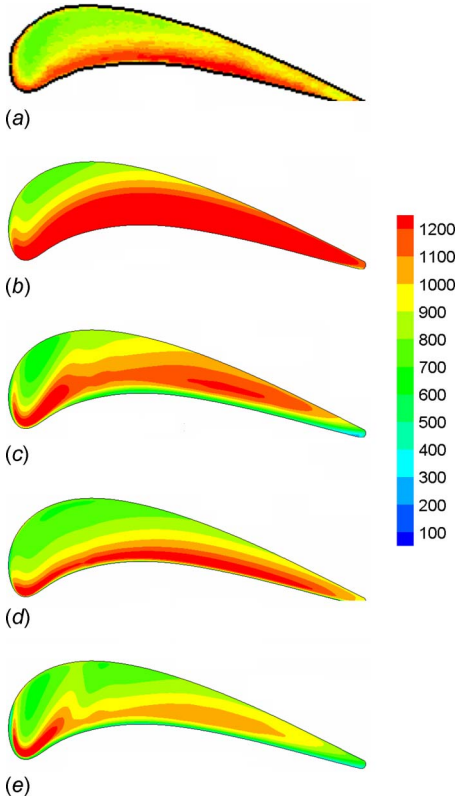

Fig. 3 Comparison of the heat transfer coefficients between experimental and predicted results: (*a*) experiment result, (*b*) standard κ-ε model, (*c*) RNG κ-ε model, (*d*) low Re κ-ω model, and (*e*) SST κ-ω model

larger than the relative leakage flow velocity, the centrifugal and Coriolis forces will bend the endwall boundary flow toward the blade tip, which blocks the development of the leakage flow in the tip gap. For the DSSS case, since a mass of gas enters the suction side through the gap, the leakage vortex has already occurred at

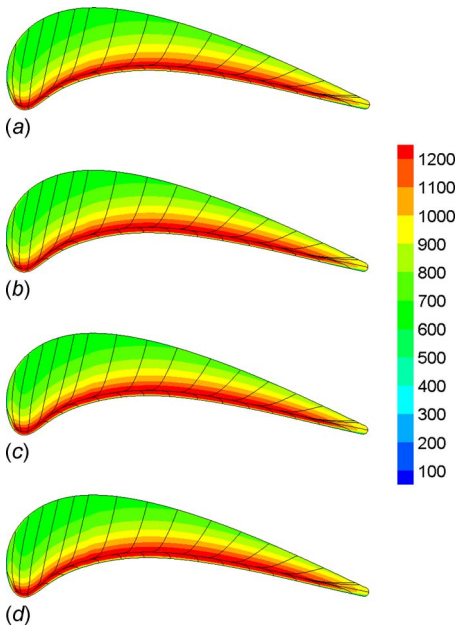

Fig. 4 Heat transfer coefficient distributions and surface streamlines on the tip: (*a*) 0.8 million, (*b*) 1.1 million, (*c*) 1.47 million, and (*d*) 2.5 million

Table 1 The averaged *h* on the blade tip

Grid node number ($\times 10^6$)	Averaged h (W/m^2 K)	Relative error (%)
0.80	912.081	−2.26
1.10	916.592	−1.78
1.47	922.435	−1.15
2.57	925.727	−0.8
Extrapolation	933.209	-

the suction surface near the tip.

From Fig. 5 it can be found that the spanwise size of the separation vortex on the tip near the pressure side is larger when the endwall relative motion exists. The orientation of the endwall relative motion is from the pressure to the suction side of the adjacent blade. This orientation is the same as that of the passage vortex near the endwall. So the endwall relative motion strengthens the passage vortex and increases the radial flow velocity on the pressure side near the tip. Also, it enlarges the spanwise size of the separation vortices.

At the 50% and 80% axial chord locations, with the increase in the pressure difference between both sides of the blade, the leakage flow becomes stronger. By comparing the DRSS case with the DSSR case, the centrifugal and Coriolis forces have little effect on the flow structure in the tip gap. While comparing the DSSR case with the DSSS case, it can be found that the endwall relative motion significantly restrains the leakage flow and reduces the circumferential size of the leakage vortices near the suction side.

Figure 6 shows the surface streamlines and the velocity magnitude contours on the middle plane between the tip and shroud in the different cases. In the DSSS case, the direction of leakage flow is nearly perpendicular to the camber line at the midaxial chord location of the blade tip. The main leakage flow occurs at the middle axial chord location from the velocity contour. However, as compared with that in the DSSS case, the streamlines turn toward the streamwise in the DSSR and DSSS cases. The highest leakage flow velocity shifts to near the trailing edge, and the velocity value also reduces. Comparing the DSSS case with the DSSR case, we can find that the endwall relative motion can significantly reduce the size of the leakage vortex.

Figure 7 shows the pressure distributions (normalized by the inlet relative total pressure) on the midspan and near the tip (98% of the blade height) of the blade surface in the flat tip cases. The effect of the blade rotation on the surface pressure distribution at the midspan is insignificant, while the effect is very strong near the tip. The pressure distribution shows the after-load characteristics due to the rotation of the blade. The effects of all of the

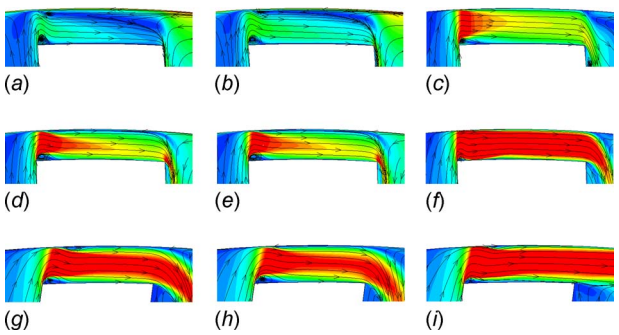

Fig. 5 The secondary flow streamlines around the flat tip at various axial locations (left is the pressure side): (*a*) DRSS, 20% axial chord, (*b*) DSSR, 20% axial chord, (*c*) DSSS, 20% axial chord, (*d*) DRSS, 50% axial chord, (*e*) DSSR, 50% axial chord, (*f*) DSSS, 50% axial chord, (*g*) DRSS, 80% axial chord, (*h*) DSSR, 80% axial chord, and (*i*) DSSS, 80% axial chord

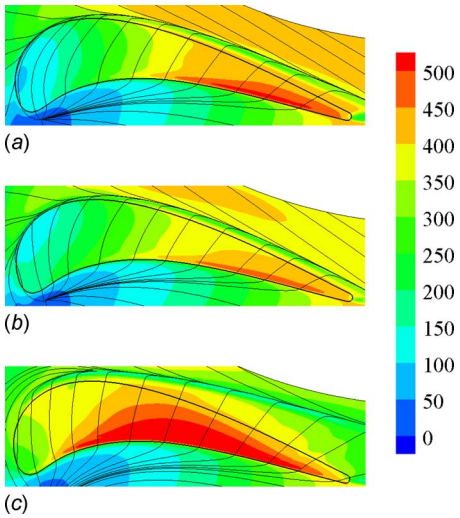

Fig. 6 Surface streamlines and velocity magnitude contours on the middle plane between the tip and shroud for the flat tip cases: (*a*) DRSS, (*b*) DSSR, and (*c*) DSSS

centrifugal force, the Coriolis force, and the endwall relative motion are clearly shown. The rotation of the blade has little effect on the pressure distribution on the pressure side, while it shows significant effect on the suction side near the tip.

The pressure contours on the shroud surface in the flat tip blade are shown in Fig. 8. For all the cases, the highest pressure occurs at the corresponding position to the blade tip near the leading edge. The lowest pressure is located at the blade tip pressure side near the trailing edge for the DRSS and DSSR cases, while it is

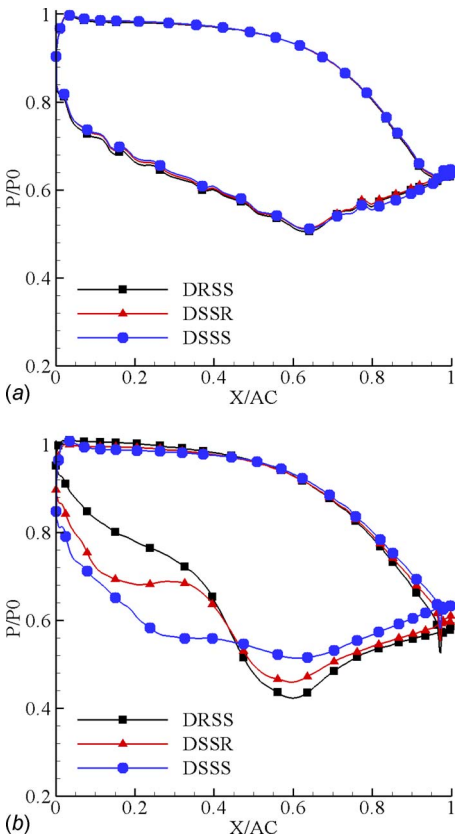

Fig. 7 The pressure distributions on the blade surface for the flat tip cases: (*a*) midspan and (*b*) near the tip

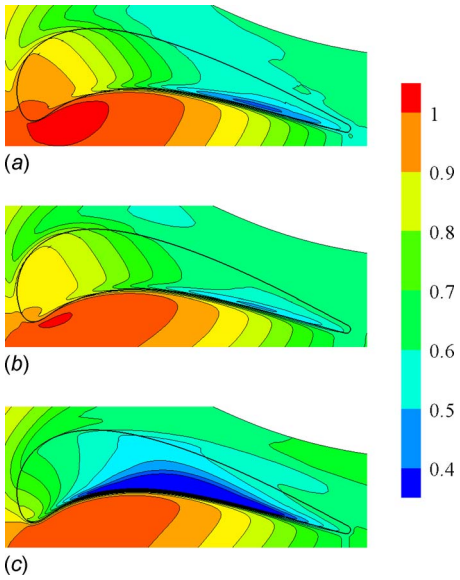

Fig. 8 The pressure contours on the shroud surface for the flat tip cases: (*a*) DRSS, (*b*) DSSR, and (*c*) DSSS

located at the blade tip pressure side near the middle axial chord for the DSSS case. For the DRSS and DSSR cases, there exist similar pressure distributions on the shroud surface. The pressure value near the blade leading edge for the DRSS case is larger than that for the DSSR case. However, the pressure is lower near the trailing edge for the DRSS case. This agrees with what is shown in Fig. 7. The comparison between the DSSR and DSSS cases indicates that the endwall relative motion has a significant effect on the pressure distribution. When the endwall relative motion exists (DSSR), the pressure near the corner at the blade tip suction side is higher than that without endwall relative motion. The reason is that for the DSSR case the boundary layer on the shroud surface has the tangential velocity component from the suction to pressure side of the blade. It blocks the leakage flow and results in the pressure increase at the exit of the tip gap. Also, for the DSSS case, the lowest pressure area shifts to the middle axial chord location, which shows the effect of the acceleration of the leakage flow in the tip gap. The pressure on the shroud surface in the DSSS case is the lowest among all three cases.

Figure 9 shows the heat transfer coefficient contours on the tip for the flat tip blade. There are similar characteristics of the heat

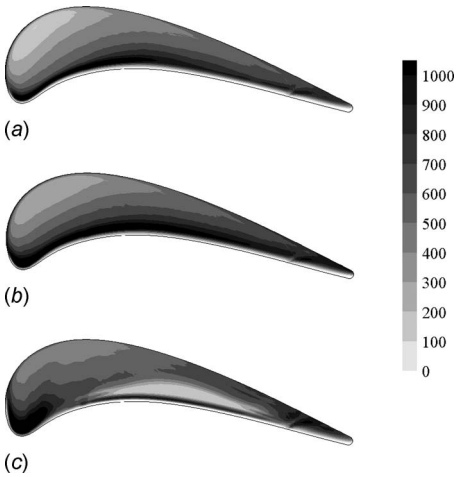

Fig. 9 The heat transfer coefficient contours on the flat tip: (*a*) DRSS, (*b*) DSSR, and (*c*) DSSS

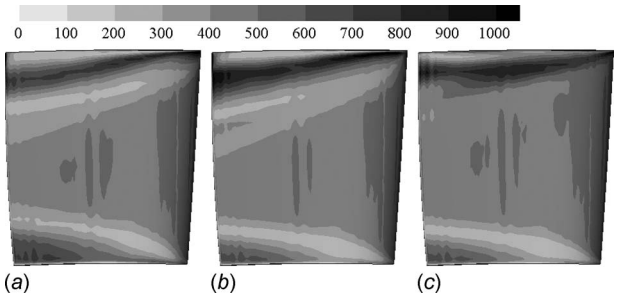

Fig. 10 The heat transfer coefficient contours on the suction surface of the flat tip blade: (*a*) DRSS, (*b*) DSSR, and (*c*) DSSS

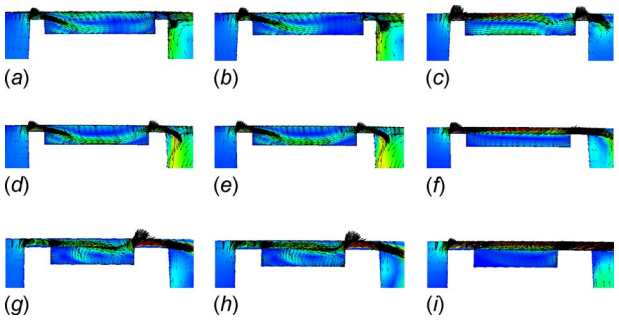

Fig. 11 View of the secondary velocity vectors around the squealer tip at various axial locations (left is the pressure side): (*a*) DRSS, 25% axial chord; (*b*) DSSR, 25% axial chord; (*c*) DSSS, 25% axial chord; (*d*) DRSS, 50% axial chord; (*e*) DSSR, 50% axial chord; (*f*) DSSS, 50% axial chord; (*g*) DRSS, 75% axial chord; (*h*) DSSR, 75% axial chord; and (*i*) DSSS, 75% axial chord

transfer distribution for the DRSS and DSSR cases. The high heat transfer region appears along the tip pressure side and the leading edge while there is a low heat transfer region on the tip suction side near the leading edge for both the DRSS and DSSR cases. When the centrifugal and Coriolis forces exist for the DRSS case, the heat transfer coefficient on the blade tip reduces compared with that for the DSSR case. For the DSSS case, there is high heat transfer coefficient region near the leading edge of the blade tip. But the lowest heat transfer coefficient region appears at the middle axial chord location near the pressure side of the blade tip. This does not agree with the conclusion of the paper [9], which may be due to the cylindrical contour of the blade tip. In this paper the cylindrical surface is employed on the tip. The convexity curvature may lead to a low heat transfer coefficient in this area [28].

The area-averaged heat transfer coefficient of the blade tip is 831.246 W/m^2 K, 908.273 W/m^2 K, and 858.207 W/m^2 K for the DRSS, DSSR, and DSSS cases, respectively. The relative motion of the endwall significantly increases the heat transfer coefficient of the blade tip, while the centrifugal and Coriolis forces reduce it.

The heat transfer coefficient contours on the blade suction surface with the flat tip are shown in Fig. 10. The characteristics of the heat transfer coefficient distribution on the suction surface are similar for all of the cases. The heat transfer coefficient near the tip increases due to the endwall relative motion by comparing the DSSR case with the DSSS case. It could be found that the low heat transfer region on the top half of the blade suction surface disappears in the DSSS case. The passage vortex near the tip is destroyed and pushed off the suction side by the strong leakage vortex in the DSSS case, which lead to the removal of the low heat transfer region. In the case of endwall relative motion, the leakage flow is weakened; however, the influence of the leakage vortex can still be found. A comparison between the DRSS and DSSR cases shows that the high heat transfer coefficient region on the suction surface near the tip reduces owing to the centrifugal force and especially the Coriolis force. The reason is that here the leakage flow passes the tip gap and turns toward the hub. So the direction of the Coriolis force is from the suction to the pressure side of the adjacent blade.

4.2 Squealer Tip. The squealer tip of the rotor blade makes the tip leakage flow even more complex. Figure 11 shows the plots of the secondary flow vectors projected on the planes normal to the axial direction at various axial locations for the three cases.

The results show that the flow structure in the tip groove for the DRSS case is very similar to that for the DSSR case. The centrifugal and Coriolis forces have insignificant effect on the structure of the leakage flow in the tip groove. A comparison between the DSSR case and the DSSS case shows that the relative motion of the endwall has a strong effect on the structure of the leakage flow in the tip groove. At the 25% axial chord location, the leakage flow is pushed to the bottom of the groove by the circumfluence vortex after entering the tip gap for the DSSR case. A further investigation about the circumfluence vortex is described in the following part. However for the DSSS case, the leakage flow does not turn into the tip groove after entering the tip gap at the 25% axial chord location at all. The same trend appears at the 50% axial chord location. Also when the endwall relative motion exists for the DSSR case the leakage flow velocity is obviously lower than that for the DSSS case at all axial chord locations.

Figure 12 shows the surface streamlines and contours of the velocity magnitude on the middle plane between the tip and shroud. For the DRSS case, the flow enters into the tip gap from the tip leading edge near the suction side and forms a circumfluence vortex in the tip gap near the endwall. This vortex will not overflow the groove until about 70% of the axial chord location. Due to the effect of the circumfluence vortex, the leakage flow turns from the tip pressure side and impinges onto the bottom of the groove. For the DSSR case, the location of the circumfluence vortex is similar to that for the DRSS case. However, the flow mainly comes from the tip leading edge. For the DSSS case, the circumfluence vortex does not appear. The leakage flow does not flow into the groove except for the region at the leading edge near the suction side.

The leakage flow forms a separation vortex near the blade tip along the suction side. A comparison between the DRSS and DSSR cases shows that there is a smaller size of leakage vortex

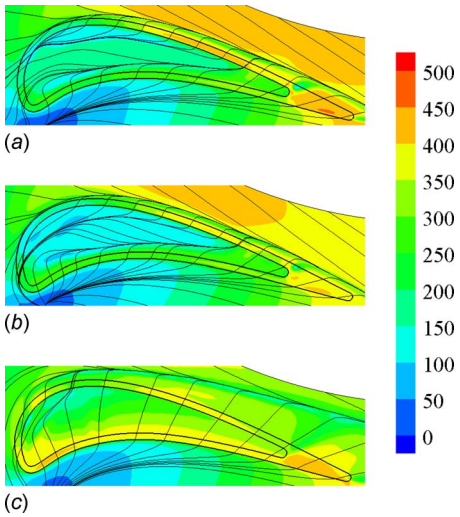

Fig. 12 The surface streamlines and velocity magnitude contours on the middle plane between the tip and shroud for the squealer tip cases: (*a*) DRSS, (*b*) DSSR, and (*c*) DSSS

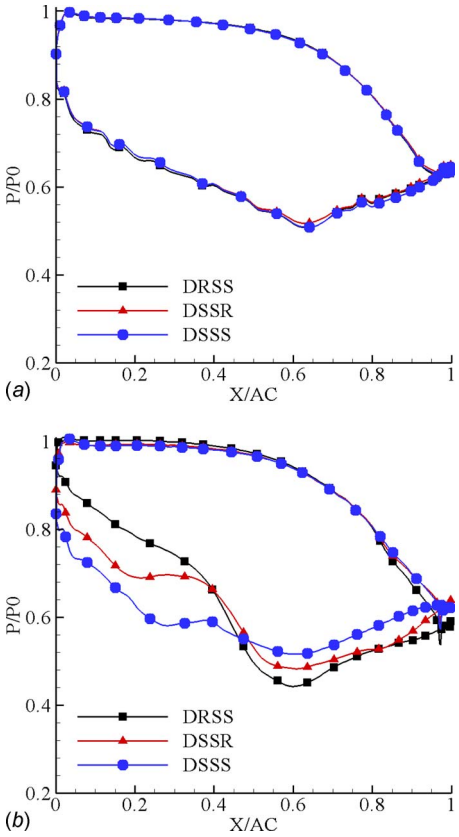

Fig. 13 The pressure distributions on the blade surface for the squealer tip cases: (*a*) midspan and (*b*) near tip

for the DSSR case. It reveals that the centrifugal and Coriolis forces can increase the tangential size of the leakage vortex. However, the effect of the centrifugal and Coriolis forces is limited. It seems that the leakage vortex has the largest size for the DSSS case. This indicates that the relative motion of the endwall can reduce the leakage flow. From the figures we can find that the velocity at the pressure side entrance of the tip gap for the DSSS case is larger than that for the other two cases. Also, for the DSSS case the velocity at the suction side exit of the tip gap is more uniform, whereas for the DRSS and DSSR cases, the leakage flow mainly concentrates on the location from the half axial chord to the training edge.

Figure 13 shows the pressure distributions on the midspan and near the tip (98% of the blade height) of the blade surface for the squealer tip cases. Similar to the effect for the flat tip cases, the effect of the blade rotation on the surface pressure distribution at the midspan is also very small, while this effect is strong near the tip. The pressure distribution indicates the after-load characteristics due to the rotation of the rotor blade.

Figure 14 shows the pressure contours on the shroud surface for the squealer tip cases. Compared with the results of the flat tip, the tip groove increases the pressure in the gap. For all cases, the highest pressure occurs at the tip suction side near the leading edge. The lowest pressure is located at the tip suction side at about 60% of the axial chord, which is the same as that shown in Fig. 13. The location of the lowest pressure shifts toward the trailing edge when the relative motion of the endwall exists. Also, all of the relative motion of the endwall, the centrifugal force, and the Coriolis force increase the pressure in the tip gap.

Figure 15 shows the contours of the heat transfer coefficient on the blade tip for the three cases. The heat transfer characteristics (both the heat transfer coefficient distribution and the value) are similar for the DRSS and DSSR cases. The effect of the centrifugal and Coriolis forces on the heat transfer of the squealer blade

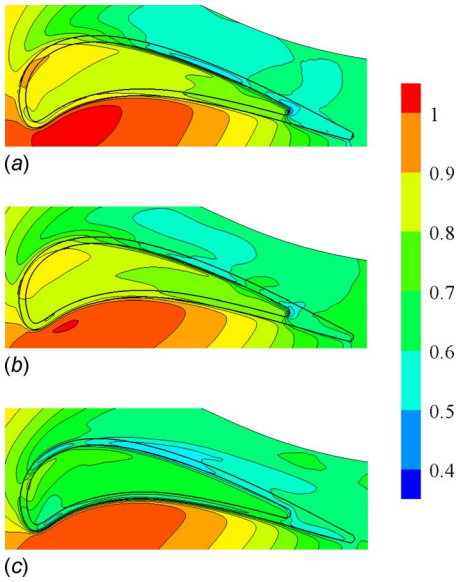

Fig. 14 The pressure contours on the shroud surface for the squealer tip cases: (*a*) DRSS, (*b*) DSSR, and (*c*) DSSS

tip is very small. However, the difference is large between the DSSR and DSSS cases. The high heat transfer coefficient region is located on the groove bottom close to the suction side for the DSSS case. While for the DSSR case, the high heat transfer coefficient region appears at the groove bottom near the pressure side, which corresponds to the impinging location of the leakage flow. The heat transfer coefficient increases due to the relative motion of the endwall.

In Fig. 15, a small break in the smooth contour can be found near the trailing edge. Also, the same problem can be found in Fig. 9 for the flat tip. As shown in Fig. 1, a single grid block is generated near the trailing edge to improve the grid quality. However it leads to the large grid aspect ratio at the interface between this block and the *O*-type grid block surrounding the groove. The large aspect ratio results in the increasing in the numerical error, especially at the corner of the tip near the pressure side, where the flow pattern is changed rapidly. Because all turbulence equations are solved by using the first order upwind advection scheme in CFX5.7, the influence is more obvious on the heat transfer that even more depends on the distribution of the turbulence.

The area-averaged heat transfer coefficient on the whole blade

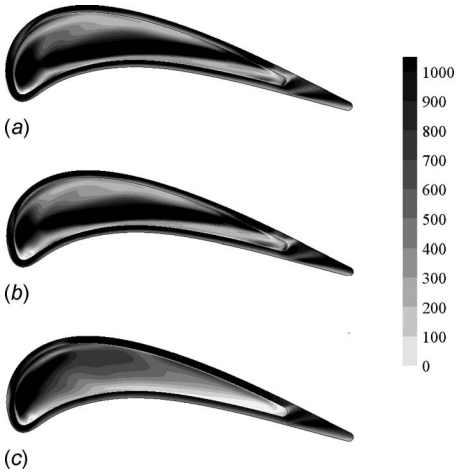

Fig. 15 The heat transfer coefficient contours on the squealer tip: (*a*) DRSS, (*b*) DSSR, and (*c*) DSSS

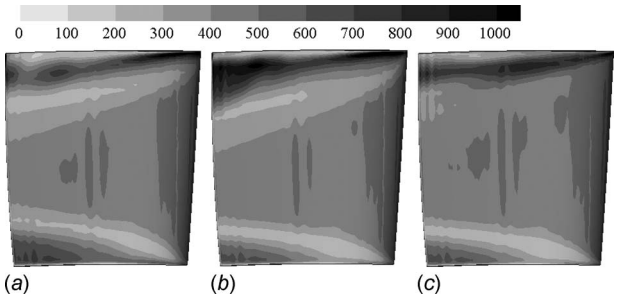

Fig. 16 The heat transfer coefficient contours on the suction surface of the squealer tip blade: (*a*) DRSS, (*b*) DSSR, and (*c*) DSSS

tip surface is 822.286 $W/m^2 K$, 824.808 $W/m^2 K$, and 748.891 $W/m^2 K$ for the DRSS, DSSR, and DSSS cases respectively. It can be found that the relative motion of the endwall can significantly increase the heat transfer coefficient on the blade tip. However the effect of the centrifugal and Coriolis forces is very small. Comparing Fig. 9 with Fig. 15, we can find that the effect of the centrifugal and Coriolis forces is small for the squealer tip but remarkable for the flat tip. As we know, the direction of the centrifugal force is irrespective of the leakage flow direction, which always has a direction along radial. However the direction of the Coriolis force depends on the leakage flow direction. In the flat tip, as the leakage flow has a large velocity along circumferential direction, the Coriolis force has a radial component, which reduces the trend of the re-attaching on the tip of the leakage flow and decreases the heat transfer coefficient on the tip. While on the squealer tip, the leakage flow turns and impinges onto the groove bottom after entering the tip gap. Since the circumferential velocity of the leakage flow reduces, the effect of the Coriolis force reduces too. For the squealer tip, the averaged heat transfer coefficient in the DRSS case is close to that in the DSSR case, which shows that the effect on the tip heat transfer may mainly come from the Coriolis force.

Figure 16 shows the contours of the heat transfer coefficient on the suction surface for the squealer tip cases. The results are similar to that for the flat tip. The heat transfer coefficient near the tip increases when the endwall relative motion exists, while it decreases due to the centrifugal and Coriolis forces.

5 Conclusions

A numerical simulation is performed to study the effect of the blade rotation on the tip leakage flow and heat transfer for the flat and squealer tip blades. The influence of the endwall relative motion, the Coriolis force, and the centrifugal force are analyzed, respectively.

The different turbulence models are validated, and the results show that the low Re k-ω turbulence model matches best with the experimental data. A grid refinement study indicates that 1.5×10^6 grid nodes can provide the solution with about 1% relative error for the flat tip blade.

For the flat tip blade, the relative motion of the endwall can reduce the leakage flow. The relative motion of the endwall, the centrifugal force, and the Coriolis force lead to the after-load characteristics of the pressure distribution near the tip. It also leads to the decrease in the leakage flow rate near the leading edge and the increase in the leakage flow rate near the trailing edge in the tip gap. The relative motion of the endwall significantly increases the averaged heat transfer coefficient on the blade tip, while the centrifugal and Coriolis forces reduce it. For the DSSS case, there exists a low heat transfer coefficient region at the tip midaxial chord location near the pressure side, which may be due to the cylindrical surface at the blade tip.

For the squealer tip blade, the flow structure in the tip groove and the heat transfer coefficient on the blade tip are mainly affected by the motion of the endwall. The effect of the centrifugal and Coriolis forces is very limited. Because of the relative motion of the endwall, a circumfluence vortex near the endwall occurs in the tip gap. The circumfluence vortex makes the leakage flow turn and impinge onto the tip groove bottom after entering the tip gap. A high heat transfer coefficient region exists on the impinging location. For the DSSS case, the high heat transfer region is located at the leading edge near the suction side of the groove bottom. While the high heat transfer coefficient region exists at the groove bottom near the pressure side due to the relative motion of the endwall for the DSSR case. The averaged heat transfer coefficient on the blade tip increases significantly due to the relative motion of the endwall. While the effect of the centrifugal and Coriolis forces on the tip averaged heat transfer coefficient is quite limited.

Acknowledgment

The authors are grateful for this work supported by National Basic Research Program (973 Program) Contract No. 2007CB210107.

References

[1] Bunker, R. S., 2001, "A Review of Turbine Blade Tip Heat Transfer," Ann. N. Y. Acad. Sci., **934**, pp. 64–79.
[2] Mayle, R. E., and Metzger, D. E., 1982, "Heat Transfer at the Tip of an Unshrouded Turbine Blade," *Proceedings of the 7th International Heat Transfer Conference*, Vol. 3, pp. 87–92.
[3] Metzger, D. E., Bunker, R. S., and Chyu, M. K., 1989, "Cavity Heat Transfer on a Transverse Grooved Wall in a Narrow Flow Channel," ASME J. Heat Transfer, **111**, pp. 73–79.
[4] Chyu, M. K., Moon, H. K., and Metzger, D. E., 1989, "Heat Transfer in the Tip Region of Grooved Turbine Blades," ASME J. Turbomach., **111**, pp. 131–138.
[5] Bunker, R. S., Bailey, J. C., and Ameri, A. A., 2000, "Heat Transfer and Flow on the First-Stage Blade Tip of a Power Generation Gas Turbine: Part 1—Experimental Results," ASME J. Turbomach., **122**, pp. 263–271.
[6] Azad, G. S., Han, J. C., Teng, S., and Boyle, R. J., 2000, "Heat Transfer and Pressure Distributions on a Gas Turbine Blade Tip," ASME J. Turbomach., **122**, pp. 717–724.
[7] Azad, G. S., Han, J. C., and Boyle, R. J., 2000, "Heat Transfer and Flow on the Squealer Tip of a Gas Turbine Blade," ASME J. Turbomach., **122**, pp. 725–732.
[8] Kwak, J. S., and Han, J. C., 2003, "Heat Transfer Coefficients on the Squealer Tip and Near Squealer Tip Regions of a Gas Turbine Blade," ASME J. Heat Transfer, **125**, pp. 669–677.
[9] Kwak, J. S., and Han, J. C., 2002, "Heat Transfer Coefficient on a Gas Turbine Blade Tip and Near Tip Regions," AIAA Paper No. 2002-3012.
[10] Newton, P. J., Lock, G. D., Krishnababu, S. K., Hodson, H. P., Dawes, W. N., Hannis, J., and Whitney, C., 2006, "Heat Transfer and Aerodynamics of Turbine Blade Tips in a Linear Cascade," ASME J. Turbomach., **128**, pp. 300–309.
[11] Nasir, H., Ekkad, S. V., Kontrovitz, D. M., Bunker, R. S., and Prakash, C., 2004, "Effect of Tip Gap and Squealer Geometry on Detailed Heat Transfer Measurements Over a High Pressure Turbine Rotor Blade Tip," ASME J. Turbomach., **126**, pp. 221–228.
[12] Ameri, A. A., and Bunker, R. S., 2000, "Heat Transfer and Flow on the First Stage Blade Tip of a Power Generation Gas Turbine Part 2: Simulation Results," ASME J. Turbomach., **122**, pp. 272–277.
[13] Yang, H. T., Acharya, S., Ekkad, S. V., Prakash, C., and Bunker, R., 2002, "Flow and Heat Transfer Predictions for a Flat-Tip Turbine Blade," ASME Paper No. GT-2002-30190.
[14] Yang, H. T., Acharya, S., Ekkad, S. V., Prakash, C., and Bunker, R., 2002, "Numerical Simulation of Flow and Heat Transfer Past a Turbine Blade With a Squealer-Tip," ASME Paper No. GT-2002-30193.
[15] Mumic, F., Eriksson, D., and Sunden, B., 2004, "On Prediction of Tip Leakage Flow and Heat Transfer in Gas Turbines," ASME Paper No. GT-2004-53448.
[16] Ameri, A. A., Steinthorsson, E., and Rigby, D. L., 1998, "Effect of Squealer Tip on Rotor Heat Transfer and Efficiency," ASME J. Turbomach., **120**(4), pp. 753–759.
[17] Yang, D. L., and Feng, Z. P., 2007, "Tip Leakage Flow and Heat Transfer Predictions for Turbine Blade," ASME Paper No. GT-2007-27728.
[18] Dunn, M. G., and Haldeman, C. W., 2000, "Time-Averaged Heat Flux for a Recessed Tip, Lip, and Platform of a Transonic Turbine Blade," ASME Paper No. 2000-GT-0197.
[19] Polanka, M. D., Clark, J. P., White, A. L., Meininger, M., and Praisner, T. J., 2003, "Turbine Tip and Shroud Heat Transfer and Loading Part B: Comparisons Between Prediction and Experiment Including Unsteady Effects," ASME GT-2003-38916.
[20] Molter, S. M., Dunn, M. G., and Haldman, C. W., 2006, "Heat-Flux Measure-

ments and Predictions for the Blade Tip Region of a High Pressure Turbine," ASME GT-2006-90048.
[21] Rhee, D. H., and Cho, H. H., 2006, "Local Heat/Mass Transfer Characteristics on a Rotating Blade With Flat Tip in Low-Speed Annular Cascade—Part I: Near Tip Surface," ASME J. Turbomach., **128**, pp. 96–109.
[22] Rhee, D. H., and Cho, H. H., 2006, "Local Heat/Mass Transfer Characteristics on a Rotating Blade With Flat Tip in Low-Speed Annular Cascade—Part II: Tip and Shroud," ASME J. Turbomach., **128**, pp. 110–119.
[23] Palafox, P., Oldfield, M. L. G., and Lagraff, J. E., 2005, "PIV Maps of Tip Leakage and Secondary Flow Fields on a Low Speed Turbine Blade Cascade With Moving Endwall," ASME Paper No. GT-2005-68189.
[24] Palafox, P., Oldfield, M. L. G., and Ireland, P. T., 2006, "Blade Tip Heat Transfer and Aerodynamics in a Large Scale Turbine Cascade With Moving Endwall," ASME Paper No. GT-2006-90425.
[25] Krishnababu, S. K., Dawes W. N., Hodson H. P., Lock, G. D., Hannis, J., and Whitney, C., 2007, "Aero-Thermal Investigation of Tip Leakage Flow in Axial Flow Turbines: Part II—Effect of Relative Casing Motion," ASME Paper No. GT-2007-27957.
[26] Timko, L. P., 1984, "Energy Efficient Engine High Pressure Turbine Component Test Performance Report," NASA Report No. CR-168289.
[27] Roache, P. J., 1994, "Perspective: A Method for Uniform Reporting of Grid Refinement Studies," ASME J. Fluids Eng., **116**, pp. 405–413.
[28] Han, J. C., Sandip, D., and Srinath, E., 2000, *Gas Turbine Heat Transfer and Cooling Technology*, Taylor & Francis, London.